GEOLOGIJA 68/2, 221-241, Ljubljana 2025

https://doi.org/10.5474/geologija.2025.009

Article

Landslides on Glaciers: from a literature collection towards a detection strategy

Plazovi na ledenikih: od pregleda literature do strategije za njihovo prepoznavanje

Gisela DOMEJ

Geological Survey of Slovenia, Dimičeva ulica 14, SI-1000 Ljubljana, Slovenia; e-mail: gisela.domej@geo-zs.si

Prejeto / Received 10. 6. 2025; Sprejeto / Accepted 25. 7. 2025; Objavljeno na spletu / Published online 25. 9. 2025

Key words: glaciers, landslides, debris, rockslides, rock avalanches, glacier dynamics
Ključne besede: ledeniki, plazovi, drobir, skalni zdrs, skalni plazovi, dinamika ledenikov

Abstract

Glacial environments are extremely sensitive to climate change and associated phenomena such as deglaciation and changes in snowfall patterns affecting the glacial mass balance globally. However, as an essential part of the Earth's water storage, glaciers are of significant importance for the geo-biologic stability.

As documented in many locations, landslides on glaciers can trigger altered glacier responses, i.e., glacial advance or glacial surges, which is approached via a literature collection in three categories: cases, inventories, and detection. This publication presents the complexity of landslides on glaciers, statistics based on the literature collection, and a possible index stacking approach towards pattern and shape recognition.

Izvleček

Ledeniška okolja so izjemno občutljiva na podnebne spremembe in z njimi povezane pojave, kot so taljenje ledenikov in spremembe v vzorcu snežnih padavin, ki vplivajo na masno bilanco ledenikov po vsem svetu. Vendar pa so ledeniki, ki predstavljajo bistveni del Zemljinih zalog vode, izjemnega pomena za geo-biološko stabilnost.

Kot je dokumentirano na številnih lokacijah, lahko plazovi na ledenikih sprožijo spremenjene ledeniške odzive, kot sta napredovanje ledenikov ali ledeniški sunki. To je obravnavano s pomočjo pregleda literature, razdeljene v tri kategorije: primeri, popisi in zaznavanje. Ta objava predstavlja kompleksnost plazov na ledenikih, statistične podatke, ki temeljijo na zbrani literaturi in možen pristop slojenja indeksov za prepoznavanje vzorcev in oblik.

Introduction

Glacial environments are endangered due to climate change and global warming, leading to general rapid deglaciation, reduced snowfall because of changes in precipitation preventing glacier growth and mass balance stability, and glacier calving at tidewater glaciers. Shrinking of ice surfaces results in a reduced albedo, which enhances the absorption of solar radiation and faster melting processes. The mechanism is of crucial importance for the Earth's water household as glaciers act as natural reservoirs, as well as for the geo-biologic balance, the sea level, climate self-regulation, and seasonality around the globe (e.g., Böhm et al., 2007).

One phenomenon that is impacting glacial dynamics is landslides on glaciers (LSGL), i.e., landslides coming to rest or traveling over glacial surfaces. This publication provides an overview of the topic, its importance explained by classic examples, and a collection of literature divided into three categories: LSGL cases, inventories, and detection. Existing databases and mapping tools are compared, and statistics on the literature collections are presented. Drawing on the publications in the category of LSGL detection, a possible index stacking approach towards LSGL pattern and shape recognition is showcased.

Landslides on glaciers

In order to approach the topic of LSGL, a correct terminology is essential, which concerns glaciers on the one hand, and the rather inconsistently used term "landslide" throughout literature on the other hand.

Glaciers are, by definition, large ice and snow masses that commonly exhibit strong dynamic down-slope behaviors caused by their weights. Glacial environments are characterized by mean annual temperatures allowing for perennial snow and ice conservation, usually around and below the freezing point. Glaciers may be distinguished by thermal regime (i.e., cold glaciers, temperate glaciers) as well as by size (i.e., ice fields/sheets, valley glaciers, cirque glaciers, piedmont glaciers, tidewater glaciers, ice caps, etc.), but categories vary throughout literature (e.g., Hagg, 2022; Huggett, 2011; Martini et al., 2001; NSDIC, 2025).

Depending on authors' preferences, however, the term "landslide" can refer to a multitude of mass movement types ranging from various forms of slides, flows, and falls (Fig. 1) typical for distinct speeds and levels of water saturation (e.g., Cruden & Varnes, 1996; Hungr et al., 2014; Hutchinson, 1968; Varnes, 1978). In glacial environments, dry mass movement types are most common – i.e., rockslides, rock avalanches, and rockfalls (Fig. 2a–b), amongst which an exact distinction is likewise difficult as one type might transform into another. For simplicity, this publication describes all concerned phenomena as "landslides".

Generally, climate change and global warming have a worldwide negative effect on the cryosphere (e.g., Bolch et al., 2012; Herreid & Pellicciotti, 2020; Rabatel et al., 2013; Sorg et al., 2012; Zemp et al., 2020) causing glacial retreat (Figure 3a) and associated processes such as, for instance, (classic) landslides and glacial lake outburst floods (GLOFS). Confirmed and predicted further global ice losses attributed to climate change draw a dramatic picture, in which glacial mass balances do not expose positive trends (e.g., Bliss et al, 2014; Shannon et al., 2019). In contrast to glacial retreat, which is considered a normal glacier response to global warming, the phenomenon of altered glacial response can be observed at different locations around the globe (Fig. 3b). Here, LSGL provide a debris cover on top of the ice, which – according to its extent – may have two effects:

- Insulation – the debris acts like a thermal insulator preserving the underlying ice masses; the debris cover, hence, slows down the process of ablation (e.g., Bessette-Kirton et al., 2018; Bull & Marangunić, 1966; Deline, 2005; Deline et al., 2015; Herreid & Pellicciotti, 2020; Shugar et al., 2012; Reznichenko et al., 2010; Reznichenko et al., 2011; Vacco et al., 2010)
- Load increase – the weight of the debris entails a vertical and/or lateral kinematic constraint and thermodynamic energy transformation; ice flow rates rise as it is considered to be proportional to driving stress to the power of three (Bons et al., 2018)

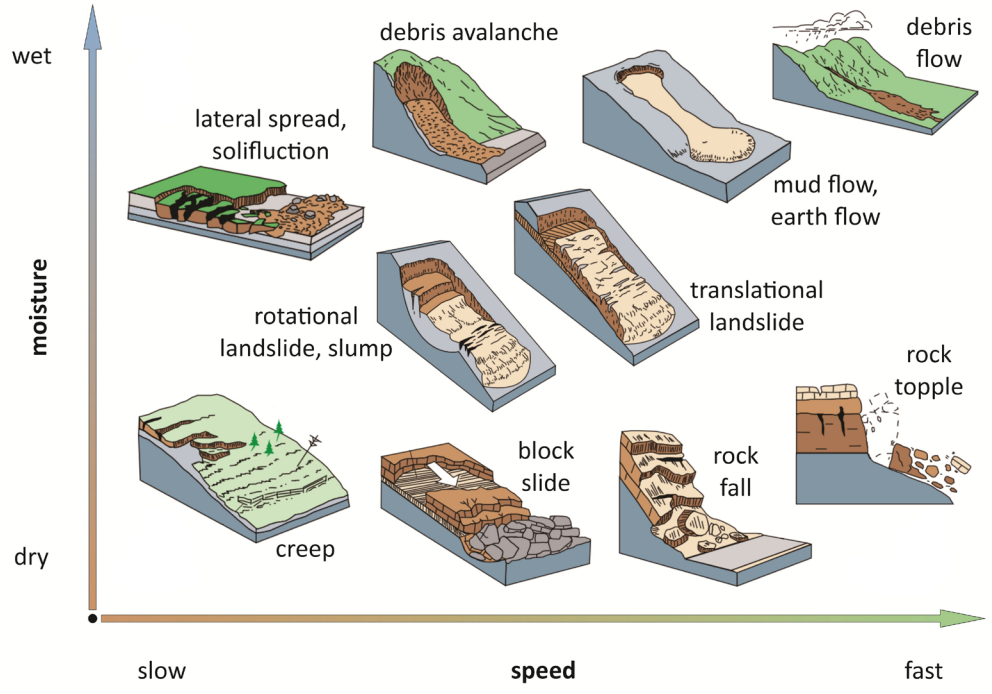

Fig. 1. Various mass movement types with gradual transition (after USGS, 2004).

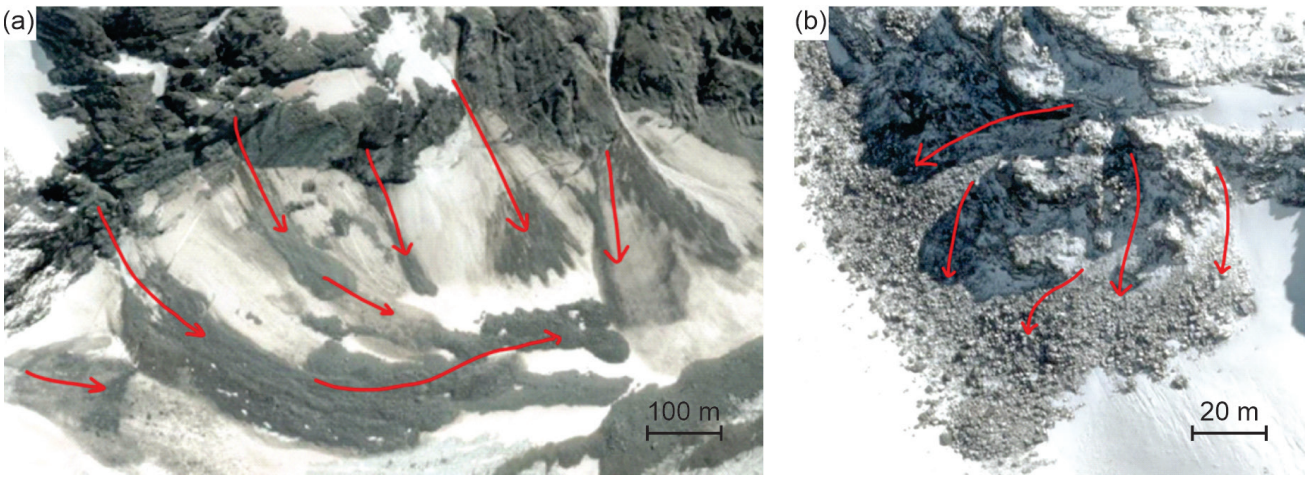

Fig. 2. Examples of rockslides and rock avalanches (**a**) and rockfalls (**b**); the exact distinction is difficult in glacial environments (photos: project internal source).

Both settings may condition glacial expansion in the direction of the least resistance (i.e., down-slope) as well as glacial advances with considerable speeds. The phenomenon might become distinctly pronounced, as LSGL often depict a far wider runout and deposit area than their non-glacial counterparts, due to considerably different friction mechanisms one ice surfaces (e.g., Delaney & Evans, 2014; Ekström & Stark, 2013).

Moreover, the formation of mixed ice-rock flows similar to debris flows is possible at glacier toes, as thermodynamic alterations might increase the formation of meltwater.

It is essential to note that besides the effect of LSGL, conditional changes in hydrological as well as thermal regimes in cold environments are known to cause rapid glacier advances or cyclic surges. They are, however, more widely discussed and documented (e.g., Björnsson, 1998; Eisen et al., 2005, Fatland & Lingle, 2002; Fowler et al., 2001; Harrison et al., 1994; Kamb et al., 1985; Kamb, 1987; Lingle & Fatland, 2003; Murray et al., 2003; Murray & Porter, 2001; Raymond, 1987) than LSGL.

The danger potential of LSGL is underlined by the event at Blatten, Switzerland, that occurred on 28th of May 2025, right at the finalization of this publication. Weathered rock from Kleines Nesthorn accumulated for years on the Birch Glacier, and a major collapse took place from 19th to 20th of May 2025, accelerating the glacial movement under additional load from several to about ten meters per day, before finally coming loose as an avalanche of millions of cubic meters of rock and ice. Large parts of the village of Blatten were destroyed and later flooded by the dammed Lonza River (Farinotti et al., 2025).

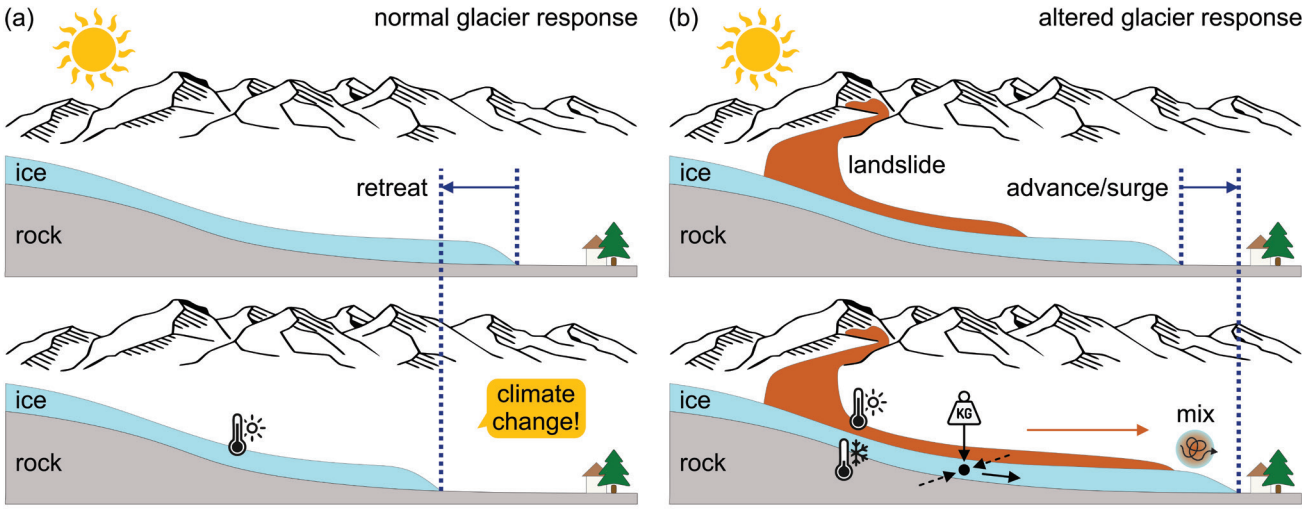

Fig. 3. Normal glacier response to climate change (**a**) and altered glacier response (**b**) due to landslide cover, resulting thermal insulation, and additional vertical load and lateral compression entailing a kinematic regime change.

Classic examples

Several prominent cases of LSGL are listed in Table 1 and shown in Figure 4a–f. It is apparent that the extent of the debris cover is not proportional to the displacement speed of the entire LSGL underlining the complexity of the phenomenon and its conditioning factors such as – amongst others – the topographic and hydrogeologic setting, local geomorphology, seasonality, and insolation, etc.

Intriguingly, one of the most striking examples of an altered glacier response to debris cover is the tailing management at the Kumtor Gold Mine in Kyrgyzstan, where starting in 1999, excavation residues were deposited on Lysii Glacier and Davidov Glacier (Jamieson et al., 2015; Evans et al., 2016). Strictly speaking, the setting is, therefore, not a classic landslide or LSGL scenario. Nonetheless, it is considered a textbook example, as glacier advances took on speeds ranging from meters to hundreds of meters per year destroying mining facilities and covering worth-to-excavate pits.

All images (Fig. 4a–f) are created with the Google Earth Engine code CataEx by Domej et al. (2025; Section 2.2.) and consist of an overlay of two layers. The RGB (red-green-blue = true-color) image components represent the extent of the Randolph Glacier Inventory 6.0 (RGI; RGI Consortium, 2017) and appear in gray scales due to rather sparse cryospheric vegetation patterns. The images underlying the RGI 6.0 polygon are false-color images carrying values between -1 and 1 of the Normalized Difference Moisture Index (previously named "water index" by Gao, 1996):

$$NDMI = \frac{NIR - SWIR1}{NIR + SWIR1} \quad \text{(Eq. 1)}$$

where ***NIR*** is the near-infrared band and ***SWIR1*** is the first short-wave infrared band of different satellite sensors.

The blue extremity (i.e., NDMI = 1) indicates very moist conditions (e.g., open waters), while the red extremity (i.e., NDMI = -1) represents extremely dry surfaces (e.g., bare rock); the latter can be mistaken for shadows.

All images (Fig. 4a–f) have the same scale emphasizing the differences in dimension of LSGL. This aspect evokes the following (non-exhaustive) series of questions, which should be the focus of data evaluation based on the here-presented literature collection throughout the runtime of the concerned scientific project (cf. Acknowledgments):

(i) location & and frequency of LSGL
- Which glaciers experience/experienced LSGL?
- Are LSGL uniformly distributed throughout glaciated regions or are they clustered?
- What is the magnitude-frequency distribution of LSGL over time?
- Is there a correlation between climate change, global warming, and a possible increase in overall landslide activity?

Table 1. Prominent cases of LSGL around the globe. The debris cover on Lysii Glacier and Davidov Glacier at the Kumtor Gold Mine, Kyrgyzstan, are artificial deposits of mine tailings (Jamieson et al., 2015; Evans et al., 2016).

Name of Glacier	Country	Occurrence between	Debris cover increase until 2022	Debris cover displacement
Morsárjökull	Iceland	2006/08 – 2007/07	3.2 km² – 7.4 km²	182 m/year
Svinafellsjökull	Iceland	2012/06 – 2013/07	± 7.7 km²	284 m/year
Lamplugh	Alaska/USA	2015/09 – 2016/08	74.1 km² – 74.3 km²	165 m/year
Kumtor Lysii Kumtor Davidov	Kyrgyzstan	deposit start 1999	[advance 1.2 km] [advance 3.2 km]	m/year to 100s of m/year
Leones 1 Leones 2	Chile	2014/03 – 2015/01 2015/01 – 2017/01	2.8 km² – 10.6 km² (combined)	500 m/year (combined)
Tasman	New Zealand	2022/01 – 2022/02	± 0.4 km²	n. d.

Table 2. Satellite image data referring to Figure 4a–f. All images originate from different collections but are categorized as Collection 2 (C2), Tier 1 (T1), and Top-of-Atmosphere (TOA). The last number sequence of the image ID indicates the date of image acquisition.

Name of Glacier	Latitude (dec°)	Longitude (dec°)	Landsat Mission	Landsat Image ID
Morsárjökull	64.09917	-16.89346	LS5	LT05_218015_20090830
Svinafellsjökull	64.01489	-16.82946	LS7	LE07_217015_20130522
Lamplugh	58.79244	-136.88199	LS8	LC08_059019_20160807
Kumtor Mine	41.877575	78.205832	LS8	LC08_148031_20140701
Leones (1 & 2)	-46.78430	-73.27296	LS8	LC08_232092_20170416
Tasman	-43.57460	170.17477	LS8	LC08_075090_20220213

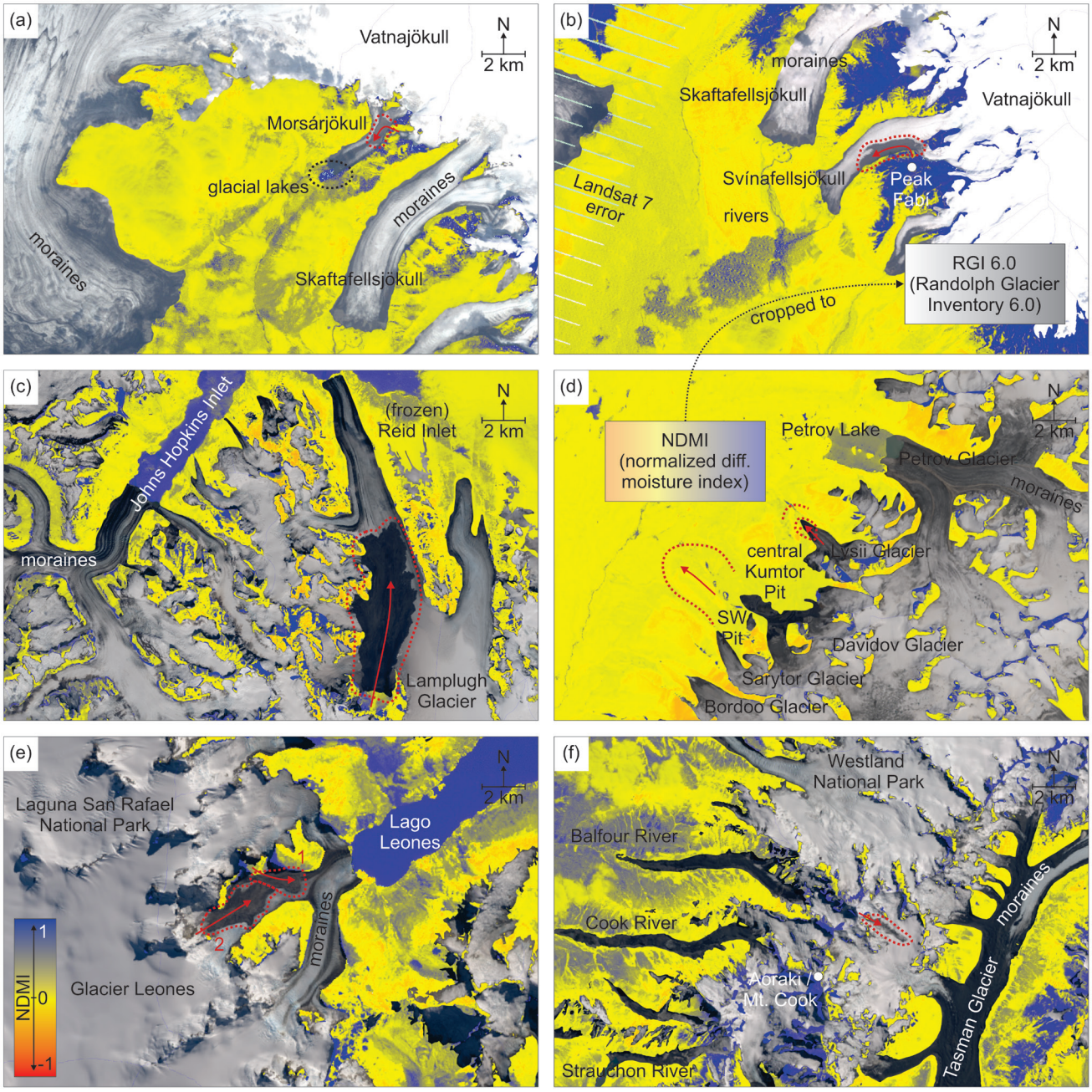

Fig. 4. Prominent cases of LSGL around the globe – on Morsárjökull, Iceland (**a**), on Svinafellsjökull, Iceland (**b**), on Lamplugh Glacier, Alaska/USA (**c**), on glaciers around the Kumtor Mine, Kyrgyzstan (**d**), on Glacier Leones, Chile (**e**), on Tasman Glacier, New Zealand (**f**). Images display NDMI exports obtained with the Google Eart Engine code CataEx (Domej et al., 2025) cropped to the RGI 6.0 (RGI Consortium, 2017) showing glaciated surfaces. Satellite image data is listed in Table 2.

(ii) processes of LSGL

- How do LSGL behave in terms of kinematics?
- How can LSGL be characterized in their dimensions?
- What mass thresholds can be considered relevant to entail an altered glacier response?
- After what time does an altered response become visible, and for how long does an altered response last?
- How can advance or cyclic surge scenarios be characterized in a dynamic, kinematic, and temporal manner?
- Are altered responses dependent on glacier regimes (i.e., cold or temperate glaciers) and/or landslide types (i.e., rockslides, rock avalanches, or rockfalls)?
- Are altered responses dependent on the extent ratio of LSGL area to glacier area, and what ratio is of critical relevance?

Literature sources and methodology

The literature collection is strongly framed by the initially very specific project goal of establishing a new global database of LSGL reaching back in time as far as (primarily) free-of-cost remote sensing

data is available. The first strategic step was, therefore, to understand from literature, which detection methods are commonly employed in the tracing process of LSGL over time. The following libraries, publishers, and platforms were searched up to March 2023 (i.e., corresponding roughly to the first year of the post-doctoral assignment of the author):

- Scopus (https://www.scopus.com/)
- Wiley Online Library (https://onlinelibrary.wiley.com/)
- ScienceDirect (https://www.sciencedirect.com/)
- Springer Nature Link (https://link.springer.com/)
- Taylor & Francis Online (https://www.tandfonline.com/)
- GeoScienceWorld (https://pubs.geoscienceworld.org/)
- ICE Virtual Library (https://www.icevirtuallibrary.com/)
- MDPI (https://www.mdpi.com/)
- ResearchGate (https://www.researchgate.net/)
- Google Scholar (https://scholar.google.com/)

For the topic of detection of LSGL, references of the publications identified as relevant were followed through until redundant. While screening publications, and with the redundant-reference approach, publications on distinct LSGL cases and LSGL inventories turned up, which were eventually collected separately (Fig. 5). It is essential to note that the collections of LSGL cases and inventories were not treated with the redundant-reference approach and, hence, reflect an overview without claiming exhaustiveness up to March 2023. Likewise, the collection of LSGL detection publications is supposedly not complete, as it is common for literature collections in general. The identified literature is listed in Appendix 2.

From Figure 5, it becomes apparent that case studies on LSGL reach back to earlier dates (even if sparsely, though), while publications on detection and inventories of LSGL significantly increased in numbers after the year 2000 when satellite imagery became considerably better and easier to access. Exemplarily, only Landsat missions of the National Aeronautics and Space Administration and the United States Geological Survey (NASA & USGS), Sentinel missions of the European Space Agency (ESA), and SPOT (French: Satellite Pour l'Observation de la Terre) of the Centre National d'Études Spatiales (CNES) are shown, reflecting only a small spectrum of spectral and radar imagery suppliers. Due to the obvious difficulty tracing LSGL back in time for reasons of image quantity and quality (Section 2.2.), the initial goal of establishing a global database of LSGL was modified into an assessment of LSGL inventories and detection methods to

(i) assemble a database from existing inventories and homogenize the data,

(ii) and study techniques to potentially fill gaps in the database.

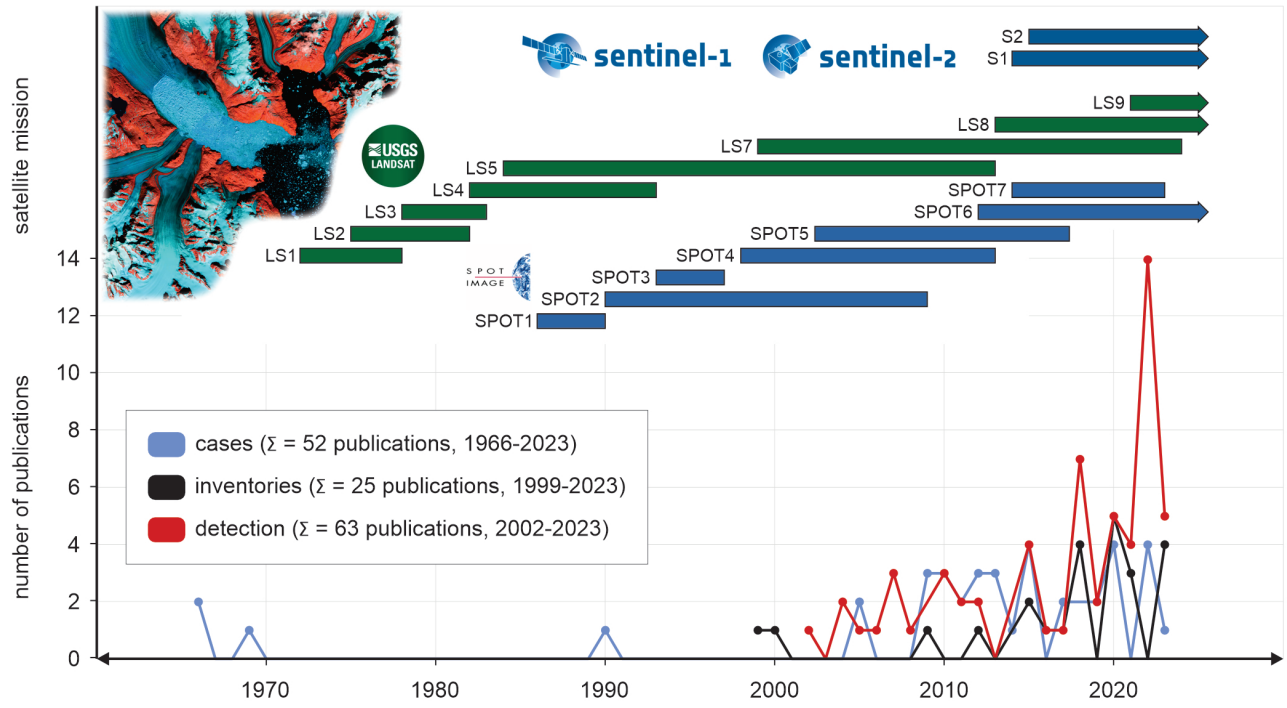

Fig. 5. Numbers of publications per year included in the here-presented literature collection and chronology of satellite missions (satellite image: after Bouchard, 2022).

Existing databases

Particularly for the task of filling gaps and detecting LSGL in areas where no inventories are established, but also to verify and complete existing inventories, several existing databases are of essential interest. As they reach back in time and/or are being updated regularly by the providing institutions and authors, they can assist in tracking both glacier extents (which condition the existence of LSGL) and debris cover across glaciers caused by LSGL.

- The World Glacier Inventory (WGI) is a global glacier database with information of more than 130,000 glaciers based on aerial photographs and maps, with most entries being non-multitemporal. By the time of establishment, it included about 85 % of the Earth's glaciers providing a static snapshot of the glaciation in the second half of the 20th century (WGMS, 1989).
- To continue the efforts of the WGI with remote sensing techniques, the initiative Global Land Ice Measurements from Space (GLIMS) was launched between the National Snow and Ice Data Center (NSIDC) and the World Glacier Monitoring Service (WGMS). GLIMS mainly relies on spectral satellite imagery such as ASTER data and several others. It globally covers more than 20,000 glaciers and 750,000 km² excluding the ice sheets in Greenland and Antarctica, with some of the glaciers having multi-temporal coverage (Kargel et al., 2014).
- Integrating GLIMS into new formats, the RGI (i.e., in all its versions) provides global coverage of single glacier outlines as polygons together with attributes and auxiliary data starting approximately from the year 2000. RGI data is available currently in its 7th version and provides a static snapshot as by the year 2023 for glaciers excluding ice sheets; it is sectioned in Global Terrestrial Network for Glaciers (GTN-G) Glacier Regions and freely available (RGI 7.0 Consortium, 2023).

A strong reference for assessing LSGL on a global scale is the dataset on Supraglacial Debris Cover provided by the GFZ (Helmholtz Centre for Geosciences) Data Services in its version 1.0 (Scherler et al., 2018b). Based on the RGI 6.0 and a remote sensing identification technique for ice and snow, Scherler et al. (2018a) mapped and analyzed the global distribution of supraglacial debris using Landsat 8 and Sentinel-2 satellite imagery with resolutions of 30 m and 10 m, respectively. The dataset includes shapefiles (SHP-file) and auxiliary data but has the drawback that areas that belong to glaciers without being ice or snow are classified as debris cover, while they could in reality be – for instance – nunataks. As the dataset draws on the RGI 6.0, information on debris cover on the ice sheets of Greenland and Antarctica is sparse. This aspect is, however, not critical for mapping LSGL, as ice sheets are usually not dissected by topographic ridges from which landslides could originate.

The tools GERALDINE, GEEDiT, and CataEx

Popular concepts and algorithms discriminating between ice, snow, and areas not containing either of them (i.e., ice-snow-free areas) are commonly based on the pixel-wise processing of satellite data combining ratios, indexes, and thresholds. Indexes refer to normalized-difference operations such as – for instance – the one for the NDMI (Equation 1); a variety of sensor band combinations result in distinct indexes, of which the most commonly used are:

- NDVI (normalized-difference vegetation index; Kriegler et al., 1969) using the NIR and red bands to differentiate open waters from healthy vegetation
- NDWI (normalized-difference water index; McFeeters, 1996) using the green and NIR bands to differentiate open waters from dry areas
- NDSI (normalized-difference snow index; Dozier, 1989) using the green and SWIR1 bands to differentiate snow and ice from bare rock and vegetation

Herreid et al. (2015), Mölg et al. (2018), and Scherler et al. (2018a) used a similar method to map ice, snow, and other areas; other authors developed comparable sequences of algorithms involving most commonly the NDVI, NDWI, and NDSI (Table A1 in the Appendix). Worth mentioning is the work of Keshri et al. (2009), who demonstrate how ice, snow, debris, and a mix of ice and debris can be distinguished in the Himalayas using the NDSI, the NDGI (normalized difference glacier index using green and red sensor bands; Keshri et al., 2009), and the NDSII (equal to the NDWI by McFeeters, 1996).

For all remote sensing-based approaches to map LSGL remains the general question, of whether areas classified as debris indeed represent LSGL; many algorithms are only designed for ice-snow-free areas, which can well locate nunataks, exposed rock cliffs, or simply areas that previously were covered by glaciers and affected by glacial

retreat. The latter discrepancy is particularly frequent when working with polygons of an older RGI version or even within the most recent version as glacial retreat can take place with striking speed. Shadow effects and cloud cover in remote sensing imagery can likewise hinder algorithms from performing properly and result in misclassifications.

Other options to outline LSGL are traditional and/or assisted mapping strategies, which can be supported by different tools such as GEEDiT (Lea, 2018) and GERALDINE (Smith et al., 2020) implemented as ready-to-run JavaScript routines in the Google Earth Engine (Gorelick et al., 2017).

GEEDiT (Google Earth Digitisation Tool) was designed by Lea (2018) to map and trace margin changes of environmental processes over time on satellite imagery of Landsat 4–8 and Sentinel-1 and -2. The complementary MaQiT (Margin Quantification Tool) allows for rapid quantification of the mapped margins (e.g., of glacier margin changes).

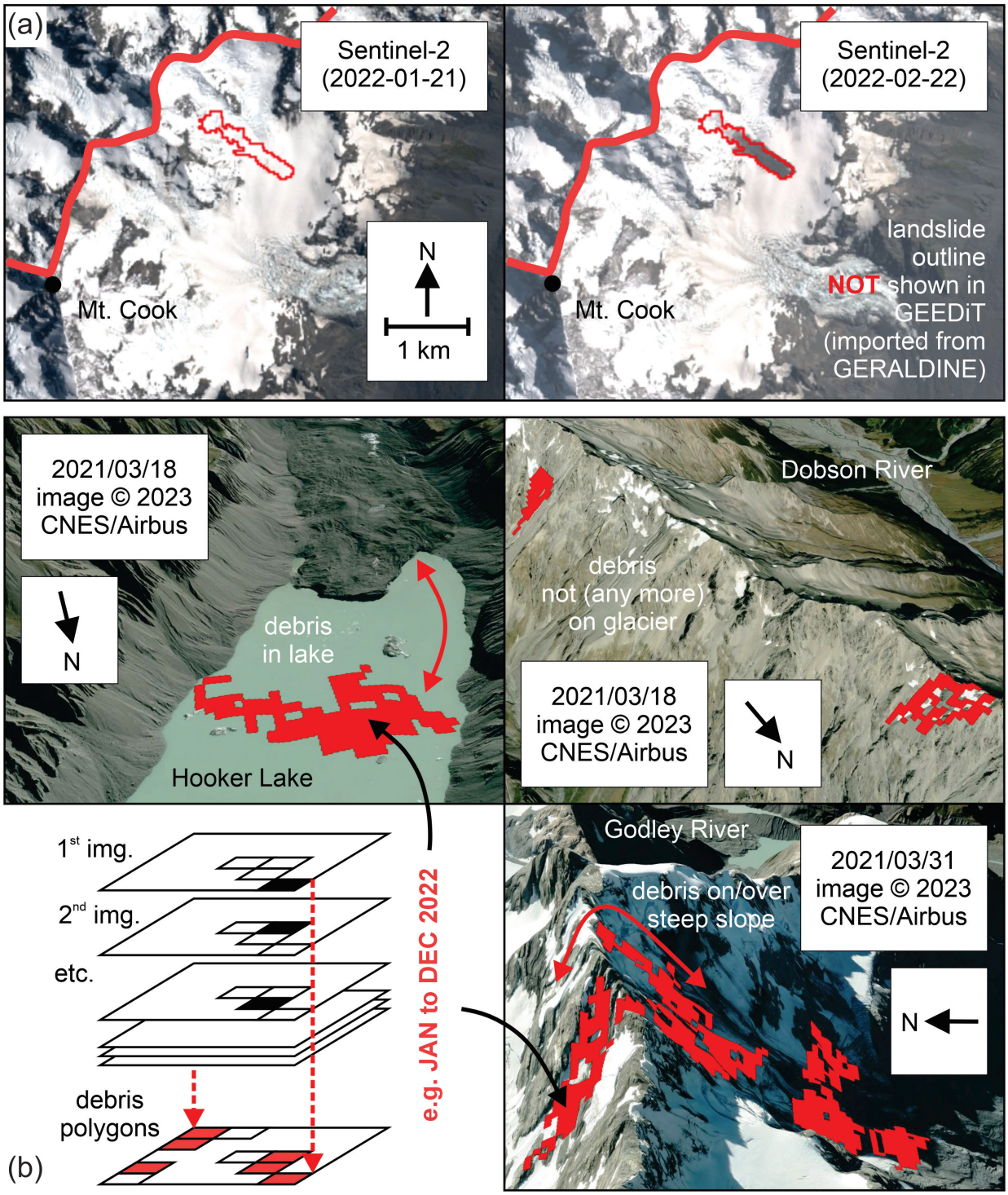

Fig. 6. Manual mapping with GEEDiT (Lea, 2018) of the LSGL on Tasman Glacier (Table 2) and assisted mapping with GERALDINE (Smith et al., 2020). Communication between GEEDiT and GERALDINE is implemented by Domej & Pluta (2022–2024).

GEEDiT alone can also be used as a catalog viewer for screening purposes to identify LSGL and their occurrence windows, which is – nonetheless – a subjective and time-consuming task (Fig. 6a).

GERALDINE (Google Earth Engine supRaglAciaL Debris INput dEtector) is likewise a JavaScript routine for the Google Earth Engine (Smith et al., 2020) that computes large debris covers on glaciers such as LSGL (with areas >0.05 km²) via a pixel-stacking and comparison approach (Fig. 6b). For a given area and timeframe, GERALDINE stacks Landsat 4–9 satellite images on top of each other to filter for pixels that fulfill the condition of "not containing debris" and turning into "containing debris" in more recent images; for this purpose, the spectral NDSI imprint is decisive with a threshold of 0.4 is below which material is classified as debris. Excluded from this algorithm are areas outside the RGI 6.0 and areas that were marked as cloudy before the launch of the algorithm (i.e., with a degree of cloudiness of 20 %). The result of each computation is a mosaic of red pixels indicative of debris input onto glaciers, which, however, is not solely sensitive to LSGL (Fig. 6b). False positives such as debris on open water bodies, debris located (not anymore) on glaciers, and/or debris on/over steep slopes are no reasonable locations for LSGL and are usually caused by a combination of reasons: (i) seasonality and glacial retreat, (ii) shadow effects, and (iii) avalanches exposing bare rock being misinterpreted as debris input, and (iv) unlikely deposit locations for LSGL in steep terrain.

To ease the process, Domej & Pluta (2022–2024) developed a code communication between both routines importing mosaics as unfilled polygons from GERALDINE into GEEDiT so that catalog screening (e.g., for the assessment of occurrence windows) would become more efficient. Furthermore, Domej & Pluta (2022–2024) introduced an image ID display into GEEDiT to keep track of distinct satellite images displaying features of particular interest or to use them in different routines where image IDs are required.

A third tool assisting in the visualization of LSGL is the Google Earth Engine code CataEx (Domej et al., 2025). Although not exclusively designed for glacial environments, Domej & Pluta (2022–2024) developed a multi-functional JavaScript routine to filter satellite image collections (i.e., Landsat and Sentinel-2 imagery), mask clouds, compute indexes and pixel-based histograms, create and visualize layers, and export images as GeoTIFFs. Besides the frequently used indexes of the NDVI, NDSI, NDWI, and NDMI, CataEx also computes the NDGI (Keshri et al., 2009), two false-color images, and several RGB images, of which one is tailored to the RGI 6.0. Figure 4a–f is an example of possible exports of CataEx via traditional GIS software (e.g., ArcGIS® Pro or QGIS).

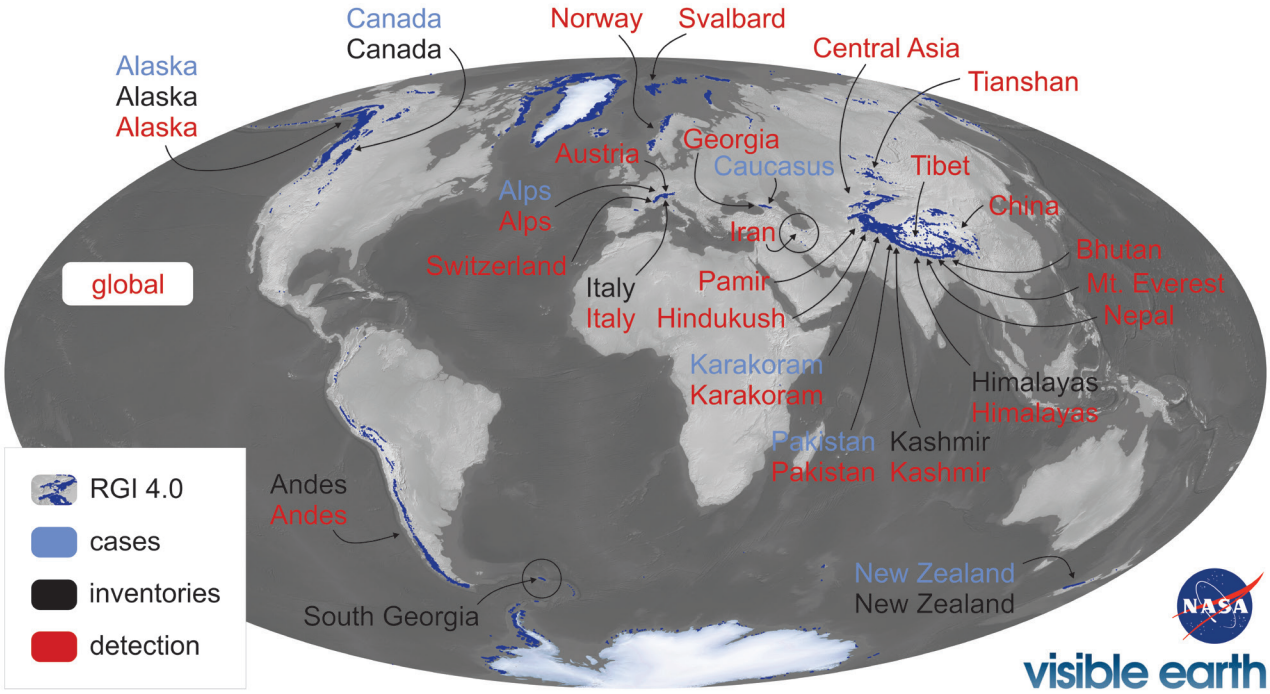

Fig. 7. Locations mentioned in publications on LSGL cases, inventories, and detection. The underlying map (after NASA visible earth, 2025) depicts the RGI 4.0 (Pfeffer et al., 2014). Distributions coincide well with the supraglacial debris cover map by Scherler et al. (2018a).

Insights into the literature collection

The collection of literature on the topic of LSGL comprises 140 publications sorted into three categories (Fig. 5): LSGL cases (#52), inventories (#25), and detection (#63). This tripartition originates from the initial ambition to (i) apprehend the worldwide distribution and/or clustering, (ii) the accomplished work on inventories and potential gaps, and (iii) strategies on how to effectively detect LSGL using satellite imagery.

A worldwide phenomenon

From an overview of collected literature, the question of global LSGL distribution can be straightforwardly answered. Referring to geographical information from the collection sections of LSGL cases and inventories, documentation of LSGL can be associated with the locations given in Figure 7. Additionally, the areas where LSGL detection was studied and/or performed are marked on the map, which is closely comparable with another map by Scherler et al. (2018a), who globally estimated supraglacial debris cover extents in percent for 1°×1° tiles from Landsat 8 imagery from 2013–2015.

Detailed quantitative and qualitative analyses on relevant contents shedding light on the questions mentioned above should be the subject of the ongoing scientific project based on this literature collection.

Detection strategies of LSGL

From Figure 8 it is apparent that both traditional and/or assisted mapping approaches as well as automated detection methods were in use over the last two decades, but within the last decade a strong tendency towards detection approaches using learning methods (Table A1 in the Appendix) became visible. Various methods appear throughout the publications and can be classified as machine learning techniques (Figure 8); they are listed in the last column of Table A1 (in the Appendix) in alphabetical order.

Several essential aspects emerge from the literature collection. Spectral satellite imagery is more popular than radar imagery, and from spectral missions, bands ranging over the visible and infrared spectrum are more frequently used than low-frequency thermal bands.

From band combinations (i.e., mostly form the green, red, NIR, and SWIR1 bands), indexes are calculated according to the example Equation 1, with the NDVI, NDSI, NDMI, and MDWI being the most recently cited in the collection of publications of LSGL detection.

Ideal information

The ideal information for the assessment of LSGL and glacial co-dynamics would consist of a clear characterization of LSGL in their spatial extent over time for comparison with the kinematic behavior of their underlying glaciers. Relevant parameters are (Fig. 9b):

L length of landslide (m)
ΔL advance of landslide (m)
G length of glacier (m)
ΔG advance of glacier (m)

$$speed_L = \frac{\Delta L - L}{\Delta t - t} \quad \text{(Eq. 2)}$$

$$speed_G = \frac{\Delta G - G}{\Delta t - t} \quad \text{(Eq. 3)}$$

where t and Δt are not necessarily the same for the landslide and the glacier but simply describe the considered time interval.

For length (and likewise width) estimations, a reference and a direction of measurement should

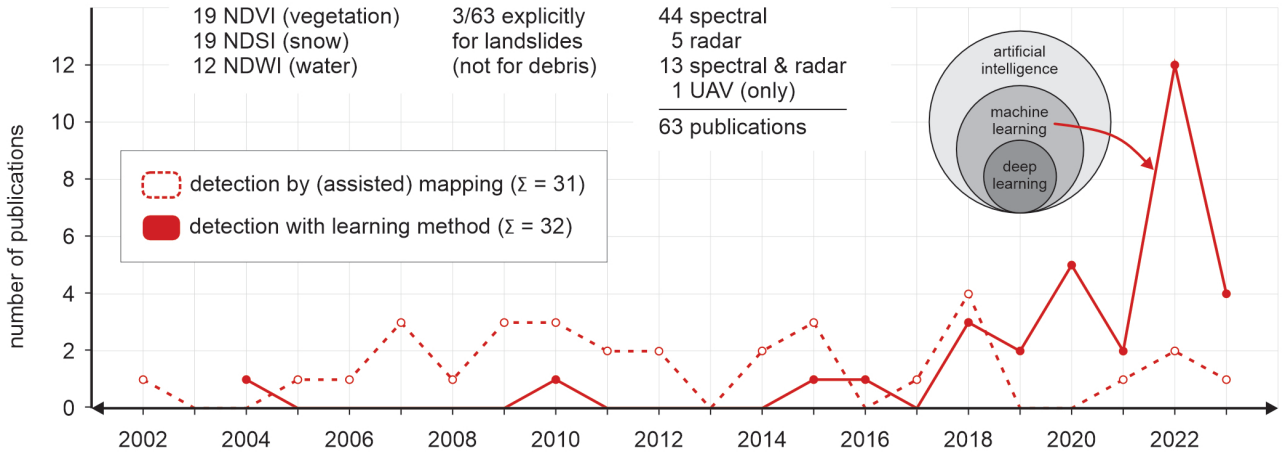

Fig. 8. Comparison of numbers of publications that used traditional and/or assisted mapping approaches for LSGL with those using automated detection with learning methods (i.e., machine learning methods).

be set, which is, however, problematic (Fig. 9b–c). Often LSGL slide into corners or hollows, which raises the question of whether an area (independently of direction-related entities) is more suitable for LSGL quantification. The question about LSGL thicknesses and volumes is even more complicated, but ultimately the most crucial for LSGL and glacial co-dynamics, as volumes give clues on additional vertical load and lateral compression entailing kinematic regime changes (Fig. 3b) and resulting enhanced ablation rates and mass balance alterations.

An aspect that significantly impedes the quantification of LSGL and glacial co-dynamics is the fact that strategies for their assessment and recorded units vary considerably between authors. For a meaningful comparison of LSGL and their effects on glaciers, the most essential step would, therefore, have to be the introduction of a standardized formats of relevant parameters and assessment strategies.

Stacking indexes strategy

Drawing on the popularity of indexes throughout different publications and acknowledging the trend towards machine learning in recent years, Domej & Pluta (2022–2024) designed a MATLAB® routine that extracts a debris mask after index stacking with the aim of exploring suitable pre-stages of datasets for pattern and shape recognition and object-based image analysis (OBIA). The ambition is to calculate debris masks, that would ideally outline shapes typical for LSGL, which could assist in training machines in pattern and shape recognition as well as assisted and automated mapping of LSGL.

As the first step, the layers containing the five indexes of the NDVI, NDSI, NDMI, NDWI, NDGI, one RGB image, and the RGI 6.0 image are exported as GeoTIFFs from the Google Earth Engine with the cote CataEx (Domej et al., 2025) for an area of interest containing an LSGL. The images each contain an n×m grid with pixel values ranging from -1 to 1 and, therefore, appear grey in any

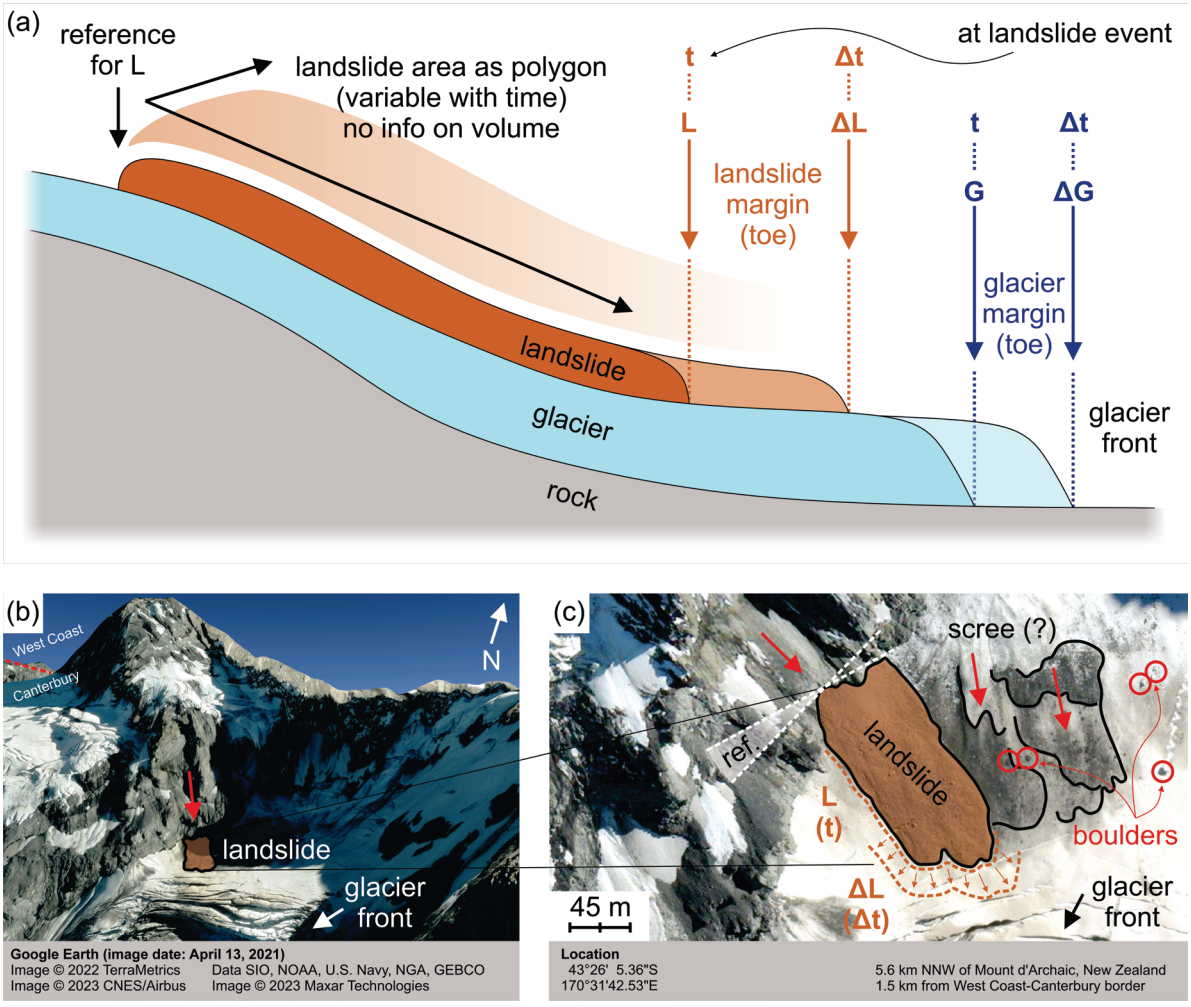

Fig. 9. Idealized LSGL sketch from which dynamic information could be calculated provided that the elevation contrast is not too pronounced (**a**), example LSGL in New Zealand (**b**), and reference discrepancies (**c**).

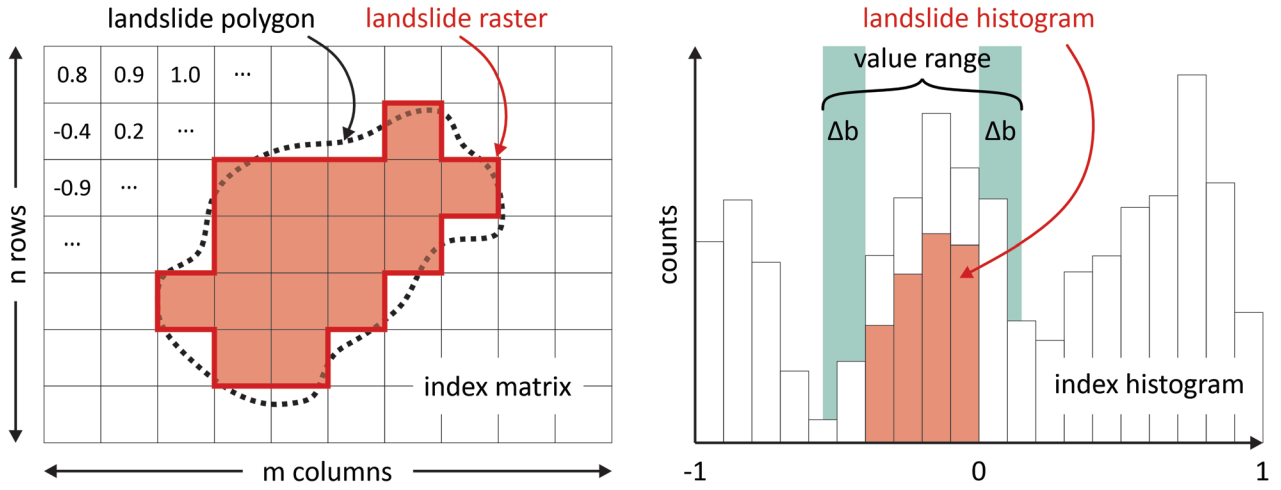

Fig. 10. Histogram calculation based on an entire index matrix and for the area included in the LSGL polygon.

software capable of displaying TIF-files. Color coding is re-applied after importing the respective grids as matrices into MATLAB®; however, color maps are different from common usage per index, as color maps in MATLAB® are not easily customizable. The RGI 6.0 image does not need a color map, as it will be used only as a stencil in the routine.

The index layer with the (subjectively) best contrast between a LSGL and the surrounding glacier and the RGB image are read in ArcGIS® Pro to outline an LSGL reference polygon, which is first rasterized and then likewise imported as TIF-file into MATLAB® where the TIF-files are treated as n×m matrices with cells holding pixel-values.

In the second step, cell value histograms are computed for all entire index matrices and for the area included in the LSGL polygon (Fig. 10).

Eventually, the MATLAB® routine performs the following sequence of operation:

1. From the histogram (per index matrix), the range of values within the LSGL polygon is retrieved (i.e., a range between min. -1 and max. 1) and a bonus (±Δb) is added to account for border cells (Fig. 10).
2. All values in cells that are not included in the identified range (including ±Δb) are eliminated (per index matrix; first four columns in Fig. 11a–c).
3. All four perforated index matrices are stacked to create a debris mask; if at least one of the four superimposed cell locations is empty, the debris mask matrix also contains an empty cell, and only if all four cell locations contain a value, the debris mask contains the value 1 and appears black (last column in Fig. 11a–c).
4. Finally, the debris mask is truncated with the RGI 6.0 matrix, to eliminate cells that do not belong to glaciers, and, hence, cannot contain debris on glaciers. It is likely, that by drawing the LSGL reference polygon manually, after the rasterization of the polygon in ArcGIS® Pro, and with the histogram bonus (±Δb), some cells enter the debris mask as "intruders"; the truncation using the RGI 6.0 can limit this problem.

The routine is somewhat functional, as the examples of three of the LSGL of Table 1 show. It must be noted that the routine is in a preliminary phase, as discussed in Section 5.

Results and discussion of the first examples of debris masks

Exemplarily, the MATLAB® routine stacking indexes and computing a debris mask was applied to Lamplugh Glacier in Alaska/USA (Fig. 11a), Glacier Leones in Chile (Fig. 11b), and Tasman Glacier in Australia (Fig. 11c). The three were chosen, as their LSGL shapes let assume straightforward, medium-successful, and difficult outlining, respectively.

For all three LSGL, the NDVI, NDSI, NDWI, NDMI, and NDGI were computed with the routine. However, the NDGI does not reveal any particular information content, as cell value ranges do not vary a lot and the image appears almost monochrome with very little perforations. The NDGI is, therefore, not displayed in Figure 11a–c, but – strictly mathematically – its matrix is included and processed in the routine alongside the other four index matrices. For all three LSGL, a bonus (±Δb) of 0.01 was added to the landslide histograms (Fig. 10).

Although indexes carry specific names, they are not limited in use to distinct contexts. For in-

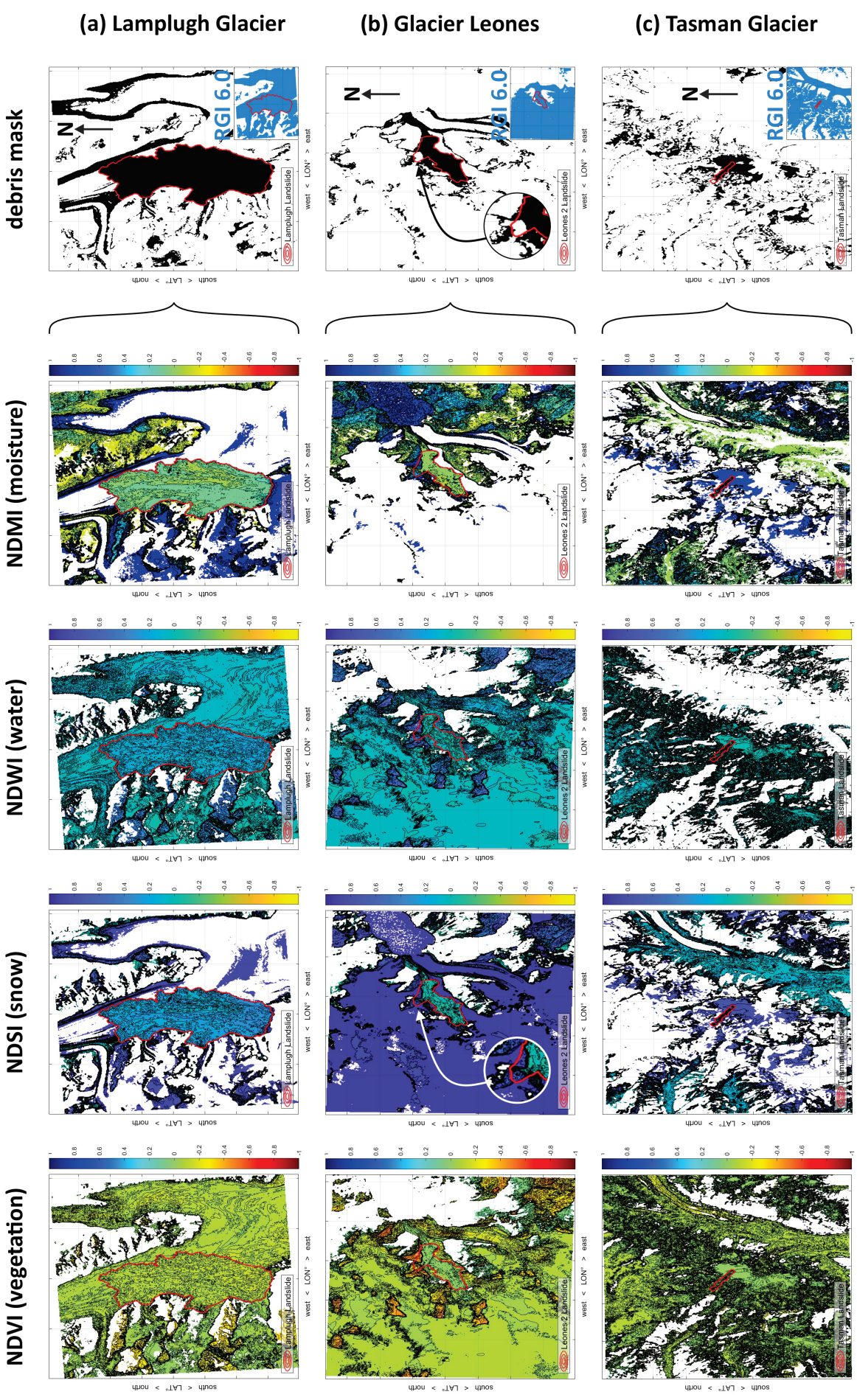

Fig. 11. Comparison of the NDVI, NDSI, NDWI, and NDMI for Lamplugh Glacier (**a**), Glacier Leones (**b**), and Tasman Glacier (**c**) and the resulting debris mask. The blue insert refers to the RGI 6.0 (RGI Consortium, 2017). Images are due north but vertically and horizontally distorted since computed and plotted in MATLAB®.

stance, the NDVI was initially developed for the discrimination between different degrees of plant health and density. Effectively, it is based on red light and NIR, from whose content conclusions can be drawn in different (e.g., glacial) environments. For the LSGL on Lamplugh Glacier, the perforated NDVI index matrix returns values around 0, which are caused by the fact that the glacier is humid compared to bare rock and open waters; in analogy, the NDWI index matrix shows a similar setting for the same reason. The index matrices of the NDSI and NDMI are likewise similar in terms of perforation due to their more pronounced sensitivity to moisture; however, the NDMI index matrix shows the best contrast between the LSGL and other surroundings. The RGI 6.0 does not significantly change the debris mask.

In addition to a similar interpretation of the setting around the two LSGL on Glacier Leones, the problem of accidental value inclusion within the LSGL polygon becomes apparent. When drawing the reference in ArcGIS® Pro, a northern corner was added to the first LSGL, which seemed to belong to it based on the RGB image. Particularly from the NDSI and NDMI index matrices, this looks, however, unlikely, and probably the additional northern corner is an artifact due to shadow effects. Also, the RGI 6.0 excludes this corner, as it is not part of a glaciated surface.

Tasman Glacier is located between cragged mountainous terrain, and rock avalanches and rockfalls are frequent and repeatedly associated with seismic activity. As the events are rather small in size compared to the LSGL on Lamplugh Glacier and Glacier Leones, it is already difficult to draw a meaningful reference polygon, which contributes to accidental value inclusion and subsequent difficulties at perforation and the creation of the debris mask.

In summary, the three examples show that by stacking index matrices, debris masks can be created, but their significance depends strongly on the correctness of the reference polygon; here, the impact of shadow and cloud effects are to be considered as well. In the course of the routine, the NDMI usually displays the strongest contrast in its index matrix, and after stacking, debris masks depict the LSGL and typical moraine structures well. The larger the LSGL and the more discriminative the surrounding environment is, the better is the routine performance; and the smaller and more cragged the terrain is, the less efficient is the debris mask as it produces too many false positives.

It is essential to keep in mind that the last column of Figure 11a–c with the coincidence of the reference polygon with the black LSGL shape cannot be seen as proof for a successful computation, as the reference polygon serves as input itself. Simply speaking, it is logical that it proves itself as LSGL. Considering, however, that the mask clearly identifies debris in the form of moraines in the immediate vicinity, it stands to reason that – at least within a certain periphery – the routine performs a correct scrutinization of debris and non-debris areas based on the spectral content of the five indexes.

In the next stage, the approach should be tested in wider areas and with a greater variety of LSGL. Moreover, the aspect of time series should be taken into account, as seasonality is a strong factor that could disturb the routine; particularly in glacial environments, snow cover can create false readings. Ideally, one or several LSGL in an area would be used as references, while some others should be (re-)identified with the debris mask according to typical shapes different from moraine deposits.

If the approach can be automated, the reference polygons could serve as learning sets for machine learning techniques in pattern and shape recognition and OBIA, offering a new strategy for mapping debris on glaciers and distinguishing LSGL from other debris covers. The latter would considerably contribute to the initial project question of whether – and if yes, how – LSGL influence glacier dynamics in terms of altered glacier responses (Fig. 3b).

Conclusion

Glacial environments are amongst the Earth's most affected by climate change. One of the many phenomena present in such environments are LSGL, which can evoke – under certain circumstances – an altered glacier response, i.e., glacial advances and/or surges, which in return can cause severe damage to life and infrastructure, as the most recent event at Blatten, Switzerland, has demonstrated in May 2025.

The causes for altered glacial responses after LSGL are the isolating effect of the debris cover protecting the underlying ice masses from melting and even benefiting ice accumulation and the increase of vertical load and lateral compression on the ice masses pushing them down-slope.

In order to apprehend the phenomenon, a comprehensive literature collection was established in three categories: LSGL cases, inventories, and detection. From those, statistics on contents of publications are presented, and drawing on the category

of LSGL detection, a strategy towards pattern and shape recognition based on index stacking is showcased. It turned out that from the NDVI, NDSI, NDWI, and NDMI a debris mask can be computed, that logically returns areas across glaciers that are covered by debris, from which patterns typical for moraines and LSGL can be distinguished. The approach is at its very initial stage, but – if developed further – it can lead to the development of machine learning techniques in pattern and shape recognition and OBIA, offering a new strategy for mapping debris on glaciers and distinguishing LSGL from other debris covers.

Funding

This work is part of the project "Global Assessment of Glacier-Landslide Interactions and Associated Geo-Hazards" (2021/42/E/ST10/00186), funded by the Polish National Science Center (NCN) and running from 2022–2027.

Data & code availability

The literature collection for this publication is available via the references given in Appendix 2. The code CataEx (Domej et al., 2025) was developed by G. D. during her post-doctoral assignment at Adam Mickiewicz University, Poznan, Poland, and can be downloaded free of charge from https://doi.org/10.5281/zenodo.8407940 (Domej et al., 2023).

References

Bessette-Kirton, E.K., Coe J.A., Zhou, W. 2018: Using Stereo Satellite Imagery to Account for Ablation, Entrainment, and Compaction in Volume Calculations for Rock Avalanches on Glaciers: Application to the 2016 Lamplugh Rock Avalanche in Glacier Bay National Park, Alaska. Journal of Geophysical Research: Earth Surface, 123/4: 622–641. https://doi.org/10.1002/2017jf004512

Björnsson, H. 1998. Hydrological characteristics of the drainage system beneath a surging glacier. Nature, 395, 6704: 771–774. https://doi.org/10.1038/27384

Bliss, A., Hock, R. & Radić, V. 2014: Global response of glacier runoff to twenty-first century climate change. Journal of Geophysical Research: Earth Surface, vol. 119/4: 717–730. https://doi.org/10.1002/2013jf002931

Böhm, R., Auer, I., Schöner, W., Hynek, B., Kroisleitner, C. & Weyss, G. 2007: Gletscher im Klimawandel - Vom Eis der Polargebiete zum Goldbergkees in den Hohen Tauern. Zentralanstalt für Meteorologie und Geodynamik, Wien: 116 p. (in German) https://austria-forum.org/web-books/gletscherimklim00de2007kfu

Bolch, T., Kulkarni A., Kaab, A., Huggel, C., Paul, F., Cogley, J.G., Frey, H., Kargel, J.S., Fujita, K., Scheel, M., Bajracharya, S. & Stoffel, M. 2012: The State and Fate of Himalayan Glaciers. Science, 336, 6079: 310–314. https://doi.org/10.1126/science.1215828

Bons, P.D., Kleiner, T., Llorens, M.G., Prior, D.J., Sachau, T., Weikusat, I. & Jansen, D. 2018: Greenland Ice Sheet: Higher Nonlinearity of Ice Flow Significantly Reduces Estimated Basal Motion. Geophysical Research Letters, 45/13: 6542–6548. https://doi.org/10.1029/2018gl078356

Bouchard, M. 2022: Landsat 9 Image of Kangerdlugssuaq Glacier, Greenland. USGS. https://www.usgs.gov/media/images/landsat-9-image-kangerdlugssuaq-glacier-greenland (accessed in June 2025)

Bull, C. & Marangunić, C. 1966: The Earthquake-Induced Slide on the Sherman Glacier, South-Central Alaska, and Its Glaciological Effects. Institute of Polar Studies, Ohio State University Publication, 108/395–408. https://eprints.lib.hokudai.ac.jp/dspace/bitstream/2115/20314/1/1_p395-408.pdf

Cruden, D.M., Varnes, D.J. 1996 : Landslide types and processes. In: Turner A.K. & Shuster R.L. (eds.): Landslides: Investigation and Mitigation. Transportation Research Board, Special Report, 247: 36–75. https://onlinepubs.trb.org/Onlinepubs/sr/sr247/sr247-003.pdf

Delaney, K.B. & Evans, S.G. 2014: The 1997 Mount Munday landslide (British Columbia) and the behaviour of rock avalanches on glacier surfaces. Landslides, 11/6: 1019–1036. https://doi.org/10.1007/s10346-013-0456-7

Deline, P. 2005: Change in surface debris cover on Mont Blanc massif glaciers after the"Little Ice Age" termination. The Holocene, 15/2: 302–309. https://doi.org/10.1191/0959683605hl809rr

Deline, P., Hewitt, K., Reznichenko, N. & Shugar, D. 2015: Rock Avalanches onto Glaciers. In: J.F. Shroder & Davies, T. (eds.): Landslide Hazards, Risks and Disasters: 263–319. https://doi.org/10.1016/b978-0-12-396452-6.00009-4

Domej, G. & Pluta, K. 2022–2024: JavaScrip and MATLAB code development for GERALDINE-GEEDiT communication, GEEDiT functionality upgrades, and preparation for OBIA integration concepts. Various unpublished reports.

Domej, G., Pluta, K. & Ewertowski, M. 2023: CataEx - Export Code for Google Earth Engine

(version 1.0). Zenodo. https://doi.org/10.5281/zenodo.8407940

Domej, G., Pluta, K. & Ewertowski, M. 2025: CataEx: a multi-task export tool for the Google Earth Engine data catalog. Environmental Modelling & Software, 183: 17 p. https://doi.org/10.1016/j.envsoft.2024.106227

Dozier, J. 1989: Spectral signature of alpine snow cover from the landsat thematic mapper. Remote Sensing of Environment, 28: 9–22. https://doi.org/10.1016/0034-4257(89)90101-6

Eisen, O., Harrison, W.D., Raymond, C.F., Echelmeyer, K.A., Bender, G.A. & Gorda, J.L.D. 2005; Variegated Glacier, Alaska, USA: a century of surges. Journal of Glaciology, 51/174: 399–406. https://doi.org/10.3189/172756505781829250

Ekström, G. & Stark, C.P. 2013: Simple Scaling of Catastrophic Landslide Dynamics. Science, 339/6126: 1416–1419. https://doi.org/10.1126/science.1232887

Evans, D.J.A., Ewertowski. M., Jamieson. S.S.R. & Orton, C. 2015: Surficial geology and geomorphology of the Kumtor Gold Mine, Kyrgyzstan: human impacts on mountain glacier landsystems. Journal of Maps, 12/5: 757–769. https://doi.org/10.1080/17445647.2015.1071720

Farinotti, D., Huss, M., Jacquemart, M., Werder, M., Knutti, R. & Seneviratne, S. 2025: Fact sheet for the now-collapsed Birchgletscher, Switzerland. ETH Zürich, 5 p. https://polybox.ethz.ch/index.php/s/eazXqWn8z6rPNwo

Fatland, D.R. & Lingle, C.S. 2002: InSAR observations of the 1993–95 Bering Glacier (Alaska, U.S.A.) surge and a surge hypothesis. Journal of Glaciology, 48/162: 439–451. https://doi.org/10.3189/172756502781831296

Fowler, A.C. 1987: A theory of glacier surges. Journal of Geophysical Research, 92/B9: 9111–9120. https://doi.org/10.1029/jb092ib09p09111

Gao, B.C. 1996: NDWI—A normalized difference water index for remote sensing of vegetation liquid water from space. Remote Sensing of Environment, 58/3: 257–266. https://doi.org/10.1016/s0034-4257(96)00067-3

Gorelick, N., Hancher, M., Dixon, M., Ilyushchenko, S., Thau, D. & Moore, R. 2017. Google Earth Engine: Planetary-scale geospatial analysis for everyone. Remote Sensing of Environment, 202: 18–27. https://doi.org/10.1016/j.rse.2017.06.031

Hagg, W. 2022. Glaciology and Glacial Geomorphology. Springer Berlin-Heidelberg, ed. 1, IX+186 p. https://doi.org/10.1007/978-3-662-64714-1

Harrison, W.D., Echelmeyer, K.A., Chacho, E.F., Raymond, C.F. & Benedict, R.J. 1994: The 1987–88 surge of West Fork Glacier, Susitna Basin, Alaska, U.S.A. Journal of Glaciology, 40/135: 241–254. https://doi.org/10.3189/s0022143000007334

Herreid, S. & Pellicciotti, F. 2020: The state of rock debris covering Earth's glaciers. Nature Geoscience, 13/9: 621–627. https://doi.org/10.1038/s41561-020-0615-0

Herreid, S., Pellicciotti, F., Ayala, A., Chesnokova, A., Kienholz, C., Shea, J. & Shrestha, A. 2015: Satellite observations show no net change in the percentage of supraglacial debris-covered area in northern Pakistan from 1977 to 2014. Journal of Glaciology, 61/227: 524–536. https://doi.org/10.3189/2015jog14j227

Huggett, R.J. 2011: Fundamentals of Geomorphology (Routledge Fundamentals of Physical Geography. Routledge, ed. 3: 536 p. https://sudartomas.wordpress.com/wp-content/uploads/2012/11/fundamentalsofgeomorphology_routledgefundamentalsofphysicalgeography.pdf

Hungr, O., Leroueil, S. & Picarelli, L. 2014: The Varnes classification of landslide types, an update. Landslides, 11: 167–194. https://doi.org/10.1007/s10346-013-0436-y

Hutchinson, J.N. 1968. Mass movement. In: Fairbridge R.W. (ed.): Encyclopedia of Geomorphology. Reinhold Publishers, 688–695.

Jamieson, S.S.R., Ewertowski, M.W. & Evans, D.J.A. 2015: Rapid advance of two mountain glaciers in response to mine-related debris loading. Journal of Geophysical Research: Earth Surface, 120/7: 1418–1435. https://doi.org/10.1002/2015jf003504

Kamb, B. 1987: Glacier surge mechanism based on linked cavity configuration of the basal water conduit system. Journal of Geophysical Research, 92/B9: 9083–9100. https://doi.org/10.1029/jb092ib09p09083

Kamb, B., Raymond, C.F., Harrison, W.D., Engelhardt, H., Echelmeyer, K.A., Humphrey, N., Brugman, M.M. & Pfeffer, T. 1985: Glacier Surge Mechanism: 1982–1983 Surge of Variegated Glacier, Alaska. Science, 22/, 4686: 469–479. https://doi.org/10.1126/science.227.4686.469

Kargel, J.S., Leonard, G.J., Bishop, M.P., Kääb, A. & Raup, B.H. 2014: Global Land Ice Measurements from Space. In: Kargel J.S., Leonard G.J., Bishop M.P., Kääb, A. & Raup, B.H.

(eds.). Springer Nature, ed. 1, p. LXXIX+876 p. https://doi.org/10.1007/978-3-540-79818-7

Keshri, A., Shukla, A. & Gupta, R.P. 2009: ASTER ratio indices for supraglacial terrain mapping. International Journal of Remote Sensing, 30/2: 519–524. https://doi.org/10.1080/01431160802385459

Kriegler, F.J., Malila, W.A., Nalepka, R.F. & Richardson, W. 1969: Preprocessing transformations and their effect on multispectral recognition. In: American Meteorological Society (ed.): Proceedings of the 6th International Symposium on Remote Sensing of Environment, 97–132.

Lea, J.M. 2018: The Google Earth Engine Digitisation Tool (GEEDiT) and the Margin change Quantification Tool (MaQiT) – simple tools for the rapid mapping and quantification of changing Earth surface margins. Earth Surface Dynamics, 6/3: 551–561. https://doi.org/10.5194/esurf-6-551-2018

Lingle, C.S. & Fatland, D.R. 2003: Does englacial water storage drive temperate glacier surges? Annals of Glaciology, 36/1: 14–20. https://doi.org/10.3189/172756403781816464

Martini, I.P., Brookfield, M.E. & Sadura, S. 2001: Principles of Glacial Geomorphology and Geology. Pearson College Division, ed. 1., 381 p.

McFeeters, S.K. 1996: The use of the Normalized Difference Water Index (NDWI) in the delineation of open water features. International Journal of Remote Sensing, 17/7: 1425–1432. https://doi.org/10.1080/01431169608948714

Mölg, N., Bolch, T., Rastner, P., Strozzi, T. & Paul, F. 2018: A consistent glacier inventory for Karakoram and Pamir derived from Landsat data: distribution of debris cover and mapping challenges. Earth System Science Data, 10/4: 1807–1827. https://doi.org/10.5194/essd-10-1807-2018

Murray, T. & Porter, P.R. 2001: Basal conditions beneath a soft-bedded polythermal surge-type glacier: Bakaninbreen, Svalbard. Quaternary International, 86/1: 103–116. https://doi.org/10.1016/s1040-6182(01)00053-2

Murray, T., Strozzi, T., Luckman, A., Jiskoot, H. & Christakos, P. 2003: Is there a single surge mechanism? Contrasts in dynamics between glacier surges in Svalbard and other regions. Journal of Geophysical Research: Solid Earth, 108(B5): 15 p. https://doi.org/10.1029/2002jb001906

NASA (National Aeronautics and Space Administration) visible earth, 2025: Randolph Glacier Inventory. NASA. https://visibleearth.nasa.gov/images/83826/randolph-glacier-inventory (accessed in June 2025)

NSDIC (National Snow and Ice Data Center), 2025: Glaciers. NSDIC. https://nsidc.org/learn/parts-cryosphere/glaciers/science-glaciers (accessed in June 2025)

Pfeffer, W.T., Arendt, A.A., Bliss, A., Bolch, T., Cogley, J.G., Gardner, A.S., Hagen, J.O., Hock, R., Kaser, G., Kienholz, C., Miles, E.S., Moholdt, G., Mölg, N., Paul, F., Radić, V., Rastner, P., Raup, B.H., Rich, J. & Sharp, M.J. 2014: The Randolph Glacier Inventory: a globally complete inventory of glaciers. Journal of Glaciology, 60/21: 537–552. https://doi.org/10.3189/2014jog13j176

Rabatel, A., Francou, B., Soruco, A., Gomez, J., Cáceres, B., Ceballos, J.L., Basantes, R., Vuille, M., Sicart, J.E., Huggel, C., Scheel, M., Lejeune, Y., Arnaud, Y., Collet, M., Condom, T., Consoli, G., Favier, V., Jomelli, V., Galarraga, R. & Ginot, P. 2013: Current state of glaciers in the tropical Andes: a multi-century perspective on glacier evolution and climate change. The Cryosphere, 7/1: 81–102. https://doi.org/10.5194/tc-7-81-2013

Raymond, C.F. 1987: How do glaciers surge? A review. Journal of Geophysical Research, 92(B9): 9121–9134. https://doi.org/10.1029/jb092ib09p09121

Reznichenko, N.V., Davies, T.R.H. & Alexander, D.J. 2011: Effects of rock avalanches on glacier behaviour and moraine formation. Geomorphology, 132/3–4: 327–338. https://doi.org/10.1016/j.geomorph.2011.05.019

Reznichenko, N., Davies, T., Shulmeister, J. & McSaveney, M. 2010: Effects of debris on ice-surface melting rates: an experimental study. Journal of Glaciology, 56/197: 384–394. https://doi.org/10.3189/002214310792447725

RGI 7.0 Consortium, 2023: Randolph Glacier Inventory - A Dataset of Global Glacier Outlines, Version 7.0. NSDIC. https://doi.org/10.5067/f6jmovy5navz

RGI Consortium, 2017: Randolph Glacier Inventory - A Dataset of Global Glacier Outlines, Version 6. NSDIC. https://doi.org/10.7265/4m1f-gd79

Scherler, D., Wulf, H. & Gorelick, N. 2018a: Global Assessment of Supraglacial Debris-Cover Extents. Geophysical Research Letters, 45/21: 11798–11805. https://doi.org/10.1029/2018gl080158

Scherler, D., Wulf, H. & Gorelick, N. 2018b: Supraglacial Debris Cover. v.1.0. GFZ Data Services. https://doi.org/10.5880/GFZ.3.3.2018.005

Shannon, S., Smith, R., Wiltshire, A., Payne, T., Huss, M., Betts, R., Caesar, J., Koutroulis, A., Jones, D. & Harrison, S. 2019: Global glacier volume projections under high-end climate change scenarios. The Cryosphere, 13/1: 325–350. https://doi.org/10.5194/tc-13-325-2019

Shugar, D.H., Rabus, B.T., Clague, J.J. & Capps, D.M. 2012: The response of Black Rapids Glacier, Alaska, to the Denali earthquake rock avalanches. Journal of Geophysical Research: Earth Surface, 117/F1: 14 p. https://doi.org/10.1029/2011jf002011

Smith, W.D., Dunning, S.A., Brough, S., Ross, N. & Telling, J. 2020: GERALDINE (Google Earth Engine supRaglAciaL Debris INput dEtector): a new tool for identifying and monitoring supraglacial landslide inputs. Earth Surface Dynamics, 8/4: 1053–1065. https://doi.org/10.5194/esurf-8-1053-2020

Sorg, A., Bolch, T., Stoffel, M., Solomina, O. & Beniston, M. 2012: Climate change impacts on glaciers and runoff in Tien Shan (Central Asia). Nature Climate Change, 2/10: 725–731. https://doi.org/10.1038/nclimate1592

USGS (United States Geological Survey), 2004: Landslide Types and Processes. USGS Fact Sheet, no. 2004-3072(-), 4 p. https://pubs.usgs.gov/fs/2004/3072/

Vacco D.A., Alley R.B. & Pollard D. 2010: Glacial advance and stagnation caused by rock avalanches. Earth and Planetary Science Letters, 294/1–2: 123–130. https://doi.org/10.1016/j.epsl.2010.03.019

Varnes, D.J. 1978: Slope Movement Types and Processes. In: Schuster, R.L. & Krizek, R.J. (eds.): Landslides, Analysis and Control. Transportation Research Board, Special Report, 176: 11–33.

WGMS (World Glacier Monitoring Service), 1989: World Glacier Inventory, status 1988 (p. 459). IAHS/UNEP/UNESCO. https://wgms.ch/downloads/wgi_1988_small.pdf

Zemp, M., Gärtner-Roer, I., Nussbaumer, S. U., Bannwart, J., Rastner, P., Paul, F. & Hoelzle, M. 2020: Global Glacier Change Bulletin, 3 (2016–2017). WGMS, 3: 289. https://wgms.ch/downloads/WGMS_GGCB_03.pdf

APPENDIX

Appendix 1

Year	Author(s)	Target area	Debris type	Indexes (mentioned)	Image type	Mapping approach	Method(s)
2023	**Ganerød** et al.	Norway	LS	NDVI	SP & RAD	LM	CCDC, CNN, U-Net
2023	**Khan** et al.	Pakistan	D	NDVI, NDWI	SP	LM	CNN, RF, SVM
2023	**Panwar & Singh**[G:D:S]	Himalayas	D		RAD	LM	DNN, SVM
2023	**Peng** et al.	China	D	NDVI, NDSI, NDWI	SP	LM	LGT & LGCB
2023	**Sharma** et al.	Himalayas	D	NDVI, NDWI, [...]	RAD	assisted	
2022	**Barella** et al.	Alps	D		SP & RAD	LM	SVM
2022	**Hu** et al.	Tibet	D	snow, cloud	SP	LM	RF
2022	**Kaushik** et al.	Himalayas, Karakoram	D		SP	LM	ANN
2022	**Lin** et al.	China	D	NDSI	SP	LM	ANN, CNN, OBIA, [...]
2022	**Lindsay** et al.	Norway	LS	NDVI	SP & RAD	assisted	
2022	**Lu** et al.	Tibet	D	NDVI, NDSI, NDWI	SP & RAD	LM	RF
2022	**Mitkari** et al.	Himalayas	D	NDWI, [...]	SP	LM	OBIA
2022	**Sharda** et al.	Karakoram	D	NDSI	SP	LM	[...]
2022	**Shukla** et al.	Himalayas	D	NDSI	SP	mapping	
2022	**Sood** et al.[G:D:S]	Himalayas	D	NDSI	SP	LM	ANN, U-Net
2022	**Tian** et al.	Pamir	D		SP	LM	U-Net
2022	**Xie** et al. (a & b)	Himalayas, Karakoram	D	NDVI, water	SP	LM	CNN
2022	**Yao** et al.	Tibet	D		RAD	LM	SVM, [...]
2021	**Holobâcă** et al.[G:D:nG]	Georgia	D	NDVI, NDSI	SP & RAD	assisted	
2021	**Xie** et al.	Karakoram	D	7 different	SP	LM	CNN, U-Net
2021	**Yan** et al.	Tibet	D	NDSI	SP	LM	U-Net
2020	**Alifu** et al.	Pakistan, China	D		SP & RAD	LM	RF, SVM, [...]
2020	**Barella** et al.	Italy, Austria	n. d.	snow, cloud	SP & RAD	LM	SVM
2020	**Khan** et al.	Pakistan	D	NDVI, NDSI, NDWI, [...]	SP	LM	ANN, RF, SVM
2020	**Lu** et al.	Pamir	D	NDVI, NDSI, NDWI	SP	LM	RF
2020	**Xie** et al.	Karakoram	D	NDWI, [...]	SP	LM	CNN
2019	**Yan** et al.	Tibet	D		SP	LM	U-Net
2019	**Zhang** et al.	Tibet	D	NDVI, NDSI, NDWI	SP	LM	RF
2018	**Azzoni** et al.	Italy	D		SP & UAV	mapping	

2018	**Lippl** et al.	Karakoram	D		SP & RAD	assisted	
2018	**Mölg** et al.	Karakoram, Pamir	D		SP & RAD	mapping	
2018	**Nijhawan** et al.	Himalayas	D		SP	LM	CNN, RF
2018	**Sahu & Gupta**	global	D		SP	LM	OBIA
2018	**Winsvold** et al.	Norway, Svalbard	n. d.		SP & RAD	mapping	
2018	**Xie** et al.	Himalayas, Karakoram	D		SP	LM	CNN
2017	**Huang** et al.	Tianshan	D		SP & RAD	mapping	
2016	**Kraajenbrink** et al.	Nepal	D	NDWI, blue index	UAV	LM	OBIA
2015	**Alifu** et al.	China	D	NDSI	SP	mapping	
2015	**Khan** et al.[G:D:S]	Himalayas, Karakoram, Hindukush	D	NDSI	SP	mapping	
2015	**Robson** et al.[G:D]	Nepal	LS	NDVI, NDSI, NDWI, [...]	SP & RAD	LM	OBIA
2015	**Smith** et al.[G:D]	Central Asia	D	NDSI	SP	assisted	
2014	**Gosh** et al.	Himalayas	D	NDSI	SP	mapping	
2014	**Huang** et al.	Tienshan	D		SP & RAD	mapping	
2012	**Karimi** et al.	Iran	D		SP	mapping	
2012	**Racoviteanu & Williams**	Himalayas	D	NDVI, NDSI	SP	mapping	
2011	**Bhambri** et al.	Himalayas	D		SP	mapping	
2011	**Jiang** et al.	China	D		RAD	mapping	
2010	**Atwood** et al.	Alaska/USA	D		RAD	mapping	
2010	**Lu** et al.	Pamir	D	NDVI, NDSI, NDWI	SP	LM	CNN, RF
2010	**Shukla** et al. (a & b)	Himalayas, Kashmir	D		SP	mapping	
2009	**Keshri** et al.[I:S:D:M]	Himalayas	D	NDSI, NDGI, NDSII	SP	mapping	
2009	**Ranzi** et al.	Italy	D	NDVI	SP	mapping	
2009	**Shukla** et al.	Himalayas, Kashmir	D		SP	mapping	
2008	**Mihalcea** et al.	Italy	D		SP	mapping	
2007	**Bolch** et al.	Everest	D		SP	assisted	
2007	**Buchroithner & Bolch**	Everest	D		SP	assisted	
2007	**Suzuki** et al.	Everest, Bhutan	D	thermal resistance	SP	mapping	
2006	**Bolch & Kamp**	Tianshan, Alps	D	NDVI	SP	mapping	
2005	**Bolch** et al.	Himalayas, Andes	D		SP	mapping	
2004	**Paul** et al.	Switzerland	D	NDVI	SP	LM	ANN
2002	**Taschner & Ranzi**	Italy	D	NDVI	SP	mapping	

Table A1: Publications related to LSGL detection (#63). References are listed in Appendix 2.

Abbreviations:

LS	–	landslides explicitly
D	–	debris
SP	–	spectral imagery
RAD	–	radar imagery
UAV	–	unmanned aerial vehicle (i.e., drones)
mapping	–	traditional mapping
assisted	–	assisted mapping
LM	–	learning method (i.e., any of machine learning)
[...]	–	other elements
ANN	–	artificial neural network
CCDC	–	continuous change detection and classification
CNN	–	convolutional neural network
DNN	–	deep neural network
LGCB	–	local global GNN (graph neural network) blocks
LGT	–	local global transformer
OBIA	–	object-based image analysis
RF	–	random forest
SVM	–	support vector machine
U-Net	–	U-shaped CNN (convolutional neural network)

Footnotes on distinction algorithms:

G:D:S	–	mapping of glacier vs. debris vs. snow
G:D:nG	–	mapping of glacier vs. debris vs. no glacier
G:D	–	mapping of glacier vs. snow
I:S:D:M	–	mapping of ice vs. snow vs. debris vs. ice-debris-mix

Appendix 2

Appendix 2 is a separate document and can be downloaded as PDF.